

Modeling Dense Multimodal Interactions Between Biological Pathways and Histology for Survival Prediction

Guillaume Jaume^{1,2,3,4,§} Anurag Vaidya^{1,2,3,4,§} Richard J. Chen^{1,2,3,4} Drew F.K. Williamson^{1,2,3,4} Paul Pu Liang⁵

Faisal Mahmood^{1,2,3,4,†}

¹Department of Pathology, Brigham and Women's Hospital, Harvard Medical School, Boston, MA, USA

²Department of Pathology, Massachusetts General Hospital, Harvard Medical School, Boston, MA, USA

³Cancer Program, Broad Institute of Harvard and MIT, Cambridge, MA, USA

⁴Data Science Program, Dana-Farber/Harvard Cancer Center, Boston, MA, USA

⁵Carnegie Mellon University, Pittsburgh, PA, USA

Abstract—Integrating whole-slide images (WSIs) and bulk transcriptomics for predicting patient survival can improve our understanding of patient prognosis. However, this multimodal task is particularly challenging due to the different nature of these data: WSIs represent a very high-dimensional spatial description of a tumor, while bulk transcriptomics represent a global description of gene expression levels within that tumor. In this context, our work aims to address two key challenges: (1) how can we tokenize transcriptomics in a semantically meaningful and interpretable way?, and (2) how can we capture dense multimodal interactions between these two modalities? Specifically, we propose to learn biological pathway tokens from transcriptomics that can encode specific cellular functions. Together with histology patch tokens that encode the different morphological patterns in the WSI, we argue that they form appropriate reasoning units for downstream interpretability analyses. We propose fusing both modalities using a memory-efficient multimodal Transformer that can model interactions between pathway and histology patch tokens. Our proposed model, SURVPATH, achieves state-of-the-art performance when evaluated against both unimodal and multimodal baselines on five datasets from The Cancer Genome Atlas. Our interpretability framework identifies key multimodal prognostic factors, and, as such, can provide valuable insights into the interaction between genotype and phenotype, enabling a deeper understanding of the underlying biological mechanisms at play. We make our code public at <https://github.com/ajv012/SurvPath>.

Keywords—Computational Pathology; Multimodal learning; Survival Prediction

I. INTRODUCTION

Predicting patient prognosis is a fundamental task in computational pathology (CPATH) that aims to utilize histology whole slide images (WSIs) for automated risk assessment, patient stratification and triage, and response-to-treatment prediction [1]–[5]. Patient prognostication is often framed as a survival analysis task, in which the goal is to learn

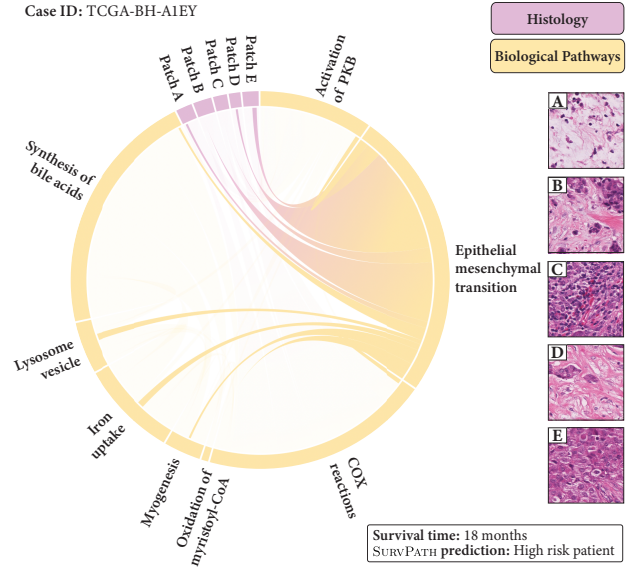


Figure 1: Our proposed architecture SURVPATH enables visualization of learned interactions via Transformer cross-attention between *biological pathways* and *morphological patterns*, here exemplified in a high-risk breast cancer patient. The chord thickness denotes attention weight. By explicitly combining *biological pathways* and *morphological patterns*, SURVPATH outperforms previous unimodal and multimodal prognostication models.

risk estimates that correctly rank the patient's time-to-event (death in the case of survival prediction) from the primary tissue slide(s) [6]–[10]. Slide-level survival prediction can be seen as a fine-grained visual recognition problem [11], in which tiny details (*e.g.* visual concepts such as tumor cells or lymphocytes [12], [13]) need to be modeled for discriminating disease stages and risk groups. As WSIs can be as large as $100,000 \times 100,000$ pixels, weakly supervised methods such as multiple instance learning (MIL) are often

[§]Equal contribution

[†]Corresponding author: Faisal Mahmood, Brigham and Women's Hospital, 75 Francis St, 8803 Boston, MA, USA. Email: faisalmahmood@bwh.harvard.edu

employed for addressing slide-level tasks. In MIL, WSIs are tokenized into small patches, from which features are extracted and then fed into pooling networks for downstream classification [14], [15].

While histology provides phenotypic information about cell types and the organization of these cell types into tissues, alternate modalities can provide complementary signals that may independently be associated with prognosis. For instance, bulk transcriptomics (the measurement of combined gene expression patterns of many cells without any spatial localization), can reveal a richer global landscape of cell types and cell states [16], [17] and has been shown to be a strong predictor of patient survival in and of itself [18]–[20]. By combining both modalities, we can integrate the global information provided by bulk transcriptomics with the spatial information from the WSI. While most existing methods adopt *late fusion* mechanisms [16], [21] (*i.e.*, fusing modality-level representations), we design an *early fusion* method that can explicitly model fine-grained cross-modal relationships between local morphological patterns and transcriptomics. In comparison with traditional computer vision and multimodal vision-language tasks [22]–[24], multimodal fusion of transcriptomics and histology presents two key technical challenges:

1. *Tokenizing transcriptomics modality*: While modalities of classical multimodal tasks (*e.g.*, image, text) can be unequivocally tokenized into object regions and word tokens [24], [25], one challenge lies in tokenizing transcriptomics in a semantically meaningful and interpretable way. As transcriptomics data is already naturally represented as a feature vector, many prior studies ignore tokenization and directly concatenate the entire feature with other modalities, which limits multimodal learning to *late fusion* operations [16], [17]. Alternatively, genes can be partitioned into coarse functional sets, representing different gene families (*e.g.*, tumor-suppressor genes and oncogenes), that can be used as tokens [26]. Nevertheless, such sets provide a rudimentary and incomplete depiction of intracellular interactions, as one gene family can be involved in different cellular functions. Consequently, they may lack semantic correspondence with fine-grained pathology features. Instead, we propose tokenizing genes according to established *biological pathways* [27]–[29]. Pathways are gene sets with known interactions that relate to *specific* cellular functions, such as the TGF- β signaling cascade, which contributes to the epithelial-mesenchymal transition in breast cancer [30]. Compared to coarse sets (*e.g.*, $N_{\mathcal{P}} = 6$ [26]), pathway-based gene grouping can yield hundreds to thousands of tokens that represent unique molecular processes ($N_{\mathcal{P}} = 331$ in our work), which we hypothesize are more suitable representations for multimodal fusion and alignment with fine-grained pathology features. In addition, as pathways represent unique cellular functions, they constitute appropriate basic reasoning units suitable for interpretability (see

Fig. 1).

2. *Capturing dense multimodal interactions*: Early fusion of histology and pathway tokens can be done with a Transformer that uses self-attention to capture pairwise similarities between all tokens [31]. However, modeling pairwise interactions between large sets of histology patch tokens (*e.g.*, $N_{\mathcal{H}} = 15,000$) and pathway tokens ($N_{\mathcal{P}} = 331$) poses scalability challenges for fusion and alignment. Due to the quadratic complexity of the Transformer attention with respect to the number of tokens, modeling all possible interactions imposes substantial computational and memory requirements. To tackle this issue, we introduce a new unified, memory-efficient attention mechanism that can successfully model patch-to-pathway, pathway-to-patch, and pathway-to-pathway interactions. Modeling these three forms of interaction is achieved by the following: (1) designing the queries, keys, and values to share parameters across token types [32], [33], and (2) simplifying the attention layer to ignore patch-to-patch interactions, which we find through experimentation to be not as effective for survival analysis. Adapting Transformer attention in such a manner leads to significant performance increase over prior works, as well as new applications for model interpretability in multimodal CPATH, especially by understanding interactions between pathways and morphological patterns.

To summarize, our contributions are (1) a transcriptomics tokenizer that leverages existing knowledge of cellular biology to generate *biological pathway* tokens; (2) SURVPATH, a memory-efficient, multimodal Transformer formulation which integrates transcriptomics and patch tokens for predicting patient survival; (3) a multi-level interpretability framework that enables deriving unimodal and cross-modal insights about the prediction; (4) a series of experiments and ablations showing the predictive power of SURVPATH, using five datasets from The Cancer Genome Atlas Program (TCGA) and benchmarked against both unimodal and multimodal fusion methods.

II. RELATED WORK

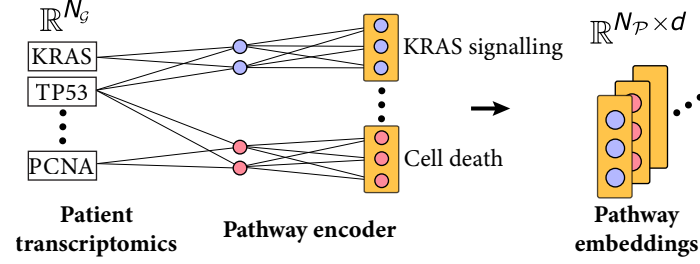
A. Survival Analysis on WSIs

Recently, several histology-based survival models utilizing MIL have been proposed [6], [34], [35]. Most contributions have been dedicated to modeling tumor heterogeneity and the tumor microenvironment. To this end, several MIL-based pooling strategies have been proposed, such as using graph neural networks to model local patch interactions [10], [36], [37], accounting for the variance between patch embeddings [38], or adopting multi-magnification patch representations [39].

B. Multimodal Transformers and Interpretability

In parallel, the use of Transformers for multimodal fusion has gained significant attention in classification and

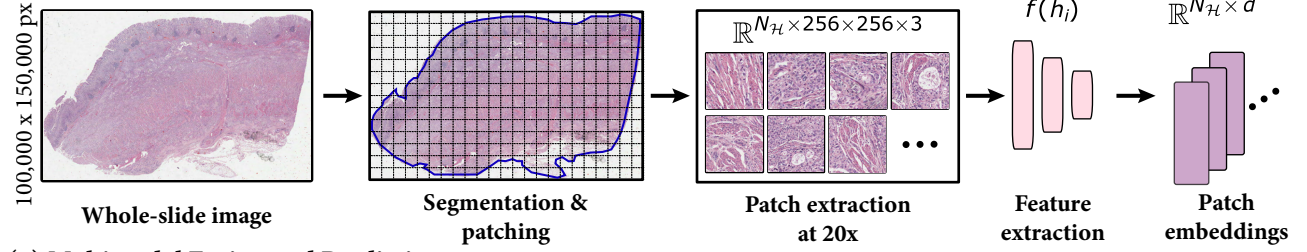
(1) Pathway Tokenizer from Transcriptomics



Legend

N_P	: Number of pathways ($N_P = 331$)
d	: Token dimension ($d = 256$)
N_G	: Number of genes ($N_G = 4,999$)
N_H	: Number of patches ($N_H = 7,000$ to $100,000$)
\otimes	: Dot product
Σ	: Average
σ	: Row-wise softmax

(2) Histology Patch Tokenizer from WSI



(3) Multimodal Fusion and Prediction

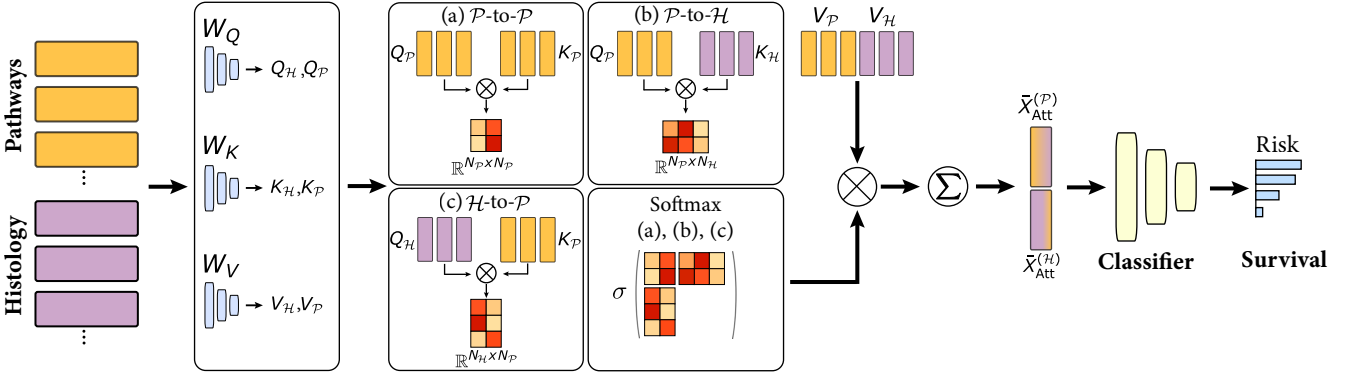


Figure 2: **Block diagram of SURVPATH.** (1) We tokenize transcriptomics into *biological pathway* tokens that are semantically meaningful, interpretable, and end-to-end learnable. (2) We further tokenize the corresponding histology whole-slide image into patch tokens using an SSL pre-trained feature extractor. (3) We combine pathway and patch tokens using a memory-efficient multimodal Transformer used for survival outcome prediction.

generative tasks [40]–[42]. Multimodal tokens can be concatenated and fed to a regular Transformer [31], [43], a hierarchical Transformer [44], or a cross-attention Transformer [45]–[47]. As the number and dimensionality of modalities increase, the typical sequence length can become too large to be fed to vanilla Transformers, hence the need for low-complexity methods. Several models have proposed re-formulations of self-attention to reduce memory requirements [32], [48]–[52], for instance, by approximating self-attention with a low-rank decomposition [49], [53], using latent bottleneck distillation [32], [33], [54], or using sparse attention patterns [48], [55]. However, none of these works have been applied to survival analysis. Recently, interpretable multimodal models or post-hoc interpretation methods [56]–[58] have also emerged as a critical area of research, especially in sensitive human-AI collaborative

decision-making scenarios such as healthcare and human-computer interactions.

C. Multimodal Survival Analysis

Multimodal integration is an important objective in cancer prognosis [5], as combining histology and omics data such as genomics or transcriptomics is the current clinical practice for many cancer types. The majority of these works employ *late fusion* mechanisms [59], [60], and mostly differ in the way modality fusion is operated. Fusion can be based on vector concatenation [61], modality-level alignment [62], bilinear pooling (*i.e.*, Kronecker product) [17], [60], or factorized bilinear pooling [16], [63].

Differently, *early fusion* mechanisms can be employed, in which cross-modal interactions between individual constituents of the input are modeled. Our work builds off

MCAT [26], which uses a cross-attention module to model the attention of histology patches (keys, values) toward gene sets (queries). However, MCAT has several limitations: (1) cross-attention being one-sided and models only patch-to-genes interactions, (2) transcriptomics tokenization using coarse sets which do not reflect actual molecular processes, and (3) significant gene overlap between sets which leads to redundant cross-attention heatmaps.

Differently, adding more modalities has also been proposed, for instance, by including radiology data [64] or clinical patient information [62].

III. METHOD

In this section, we present SURVPATH, our proposed method for multimodal survival prediction based on histology and transcriptomics. Sec. III-A presents the transcriptomics encoder to build biological pathway tokens, Sec. III-B presents the histology encoder to build patch tokens, Sec. III-C presents our Transformer-based multimodal aggregation, and Sec. III-D presents its application to survival prediction (see Fig. 2). Finally, Sec. III-E introduces our multi-level interpretability framework.

A. Pathway Tokenizer from Transcriptomics

Composing pathways: Selecting the appropriate reasoning unit for transcriptomics analysis is challenging, owing to the intricate and hierarchical nature of cellular processes. Pathways, consisting of a group of genes or subpathways involved in a particular biological process, represent a natural reasoning unit for this analysis. A comparison may be drawn to action recognition, where an action (*i.e.*, a biological pathway) can be described by a series of movements captured by sensors (*i.e.*, transcriptomics measurements of a group of genes).

Encoding pathways: Given a set of transcriptomics measurements of N_G genes, denoted as $\mathbf{g} \in \mathbb{R}^{N_G}$, and the composition of each pathway, we aim to build pathway-level tokens $\mathbf{X}^{(P)} \in \mathbb{R}^{N_P \times d}$, where d denotes the token dimension. Transcriptomics can be seen as tabular data, which can be efficiently encoded with multilayer perceptrons (MLPs). Specifically, we are learning pathway-specific weights ϕ_i , *i.e.*, $\mathbf{x}_i^{(P)} = \phi_i(\mathbf{g}_{P_i})$, where \mathbf{g}_{P_i} is the gene set present in pathway P_i . This can be viewed as learning a *sparse* multi-layer perceptron (S-MLP) [65]–[67] that maps transcriptomics $\mathbf{g} \in \mathbb{R}^{N_G}$ to tokens $\mathbf{x}^{(P)} \in \mathbb{R}^{N_P d}$. The network sparsity is controlled by the gene-to-pathway connectivity embedded in the S-MLP weights. By simply reshaping $\mathbf{x}^{(P)} \in \mathbb{R}^{N_P d}$ into $\mathbf{X}^{(P)} \in \mathbb{R}^{N_P \times d}$, we define pathway tokens that can be used by the Transformer. Each pathway token corresponds to a deep representation of the gene-level transcriptomics that comprises it, which is both (1) interpretable as it encodes a specific biological function, and (2) learnable in an end-to-end fashion with respect to the prediction task.

B. Histology Patch Tokenizer from WSIs

Given an input WSI, our goal is to derive low-dimensional patch-level embeddings defining patch tokens. We start by identifying tissue regions to ensure that the background, which carries no biological meaning, is disregarded. Then, we decompose the identified tissue regions into a set of N_H non-overlapping patches at $20\times$ magnification (or $\sim 0.5 \mu\text{m}/\text{pixel}$ resolution), that we denote as $\mathbf{H} = \{\mathbf{h}_1, \dots, \mathbf{h}_{N_H}\}$. Due to the large number of patches per WSI (*e.g.*, can be $> 50,000$ patches or 78 GB as floats), patch embeddings need to be extracted prior to model training to reduce the overall memory requirements. Formally, we employ a pre-trained feature extractor $f(\cdot)$ to map each patch \mathbf{h}_i into a patch embedding as $\mathbf{x}_i^{(H)} = f(\mathbf{h}_i)$. In this work, we use a Swin Transformer encoder that was pretrained via contrastive learning on more than 15 million pan-cancer histopathology patches [68], [69]. The resulting patch embeddings represent compressed representations of the patches (compression ratio of 256), that we further pass through a learnable linear transform to match the token dimension d , yielding patch tokens $\mathbf{X}^{(H)} \in \mathbb{R}^{N_H \times d}$.

C. Multimodal Fusion

We aim to design an early fusion mechanism that can model dense multimodal interactions between pathway and patch tokens. We employ Transformer attention [31] that can measure and aggregate pair-wise interactions between multimodal tokens. Specifically, we define a multimodal sequence by concatenating the pathway and patch tokens resulting in $(N_H + N_P)$ tokens of dimensions d , and denoted as $\mathbf{X} \in \mathbb{R}^{(N_P + N_H) \times d}$. Following the self-attention terminology [31], we define three linear projections of the tokens using learnable matrices, denoted as $\mathbf{W}_Q \in \mathbb{R}^{d \times d_q}$, $\mathbf{W}_K \in \mathbb{R}^{d \times d_k}$, and $\mathbf{W}_V \in \mathbb{R}^{d \times d_v}$ to extract the queries (\mathbf{Q}), keys (\mathbf{K}), values (\mathbf{V}), and self-attention \mathbf{A} . We set $d = d_k = d_q = d_v$. Transformer attention is then defined as:

$$\mathbf{X}_{\text{Att}} = \sigma\left(\frac{\mathbf{Q}\mathbf{K}^T}{\sqrt{d}}\right)\mathbf{V} = \begin{pmatrix} \mathbf{A}_{P \rightarrow P} & \mathbf{A}_{P \rightarrow H} \\ \mathbf{A}_{H \rightarrow P} & \mathbf{A}_{H \rightarrow H} \end{pmatrix} \begin{pmatrix} \mathbf{V}_P \\ \mathbf{V}_H \end{pmatrix} \quad (1)$$

where σ is the row-wise softmax. The term $\mathbf{Q}\mathbf{K}^T$ has memory requirements $\mathcal{O}((N_H + N_P)^2)$, which for long sequences becomes prohibitively expensive to compute. This constitutes a major bottleneck as a WSI can include more than 50,000 patches making this computation challenging on most hardware, *e.g.*, storing a $50,000 \times 50,000$ matrix requires 20 GB of RAM. Instead, we propose to decompose the multimodal Transformer attention into four intra- and cross-modality terms: (1) the intra-modal pathway self-attention encoding pathway-to-pathway interactions $\mathbf{A}_{P \rightarrow P} \in \mathbb{R}^{N_P \times N_P}$, (2) the cross-modal pathway-guided cross-attention encoding pathway-to-patch interactions $\mathbf{A}_{P \rightarrow H} \in \mathbb{R}^{N_P \times N_H}$, (3) the cross-modal histology-guided cross attention encoding patch-to-pathway interactions

tions $\mathbf{A}_{\mathcal{H} \rightarrow \mathcal{P}} \in \mathbb{R}^{N_{\mathcal{H}} \times N_{\mathcal{P}}}$, and (4) the intra-modal full histology self-attention encoding patch-to-patch interactions $\mathbf{A}_{\mathcal{H} \rightarrow \mathcal{H}} \in \mathbb{R}^{N_{\mathcal{H}} \times N_{\mathcal{H}}}$.

As the number of patch tokens is much larger than the number of pathways, *i.e.*, $N_{\mathcal{H}} \gg N_{\mathcal{P}}$, most memory requirements come from computing and storing $\mathbf{A}_{\mathcal{H} \rightarrow \mathcal{H}}$. To address this bottleneck, we approximate Transformer attention as:

$$\hat{\mathbf{X}}_{\text{Att}} = \begin{pmatrix} \mathbf{X}_{\text{Att}}^{(\mathcal{P})} \\ \hat{\mathbf{X}}_{\text{Att}}^{(\mathcal{H})} \end{pmatrix} = \sigma \left[\frac{1}{\sqrt{d}} \begin{pmatrix} \mathbf{Q}_{\mathcal{P}} \mathbf{K}_{\mathcal{P}}^T & \mathbf{Q}_{\mathcal{P}} \mathbf{K}_{\mathcal{H}}^T \\ \mathbf{Q}_{\mathcal{H}} \mathbf{K}_{\mathcal{P}}^T & -\infty \end{pmatrix} \right] \mathbf{V} \quad (2)$$

where $\mathbf{Q}_{\mathcal{P}}$ (respectively $\mathbf{K}_{\mathcal{P}}$) and $\mathbf{Q}_{\mathcal{H}}$ (respectively $\mathbf{K}_{\mathcal{H}}$) denotes the subset of pathway and histology queries and keys. Setting pre-softmax patch-to-patch interactions to $-\infty$ is equivalent to ignore these interactions. Expanding Eq. 2, we obtain that $\mathbf{X}_{\text{Att}}^{(\mathcal{P})} = \sigma \left(\frac{\mathbf{Q}_{\mathcal{P}} \mathbf{K}_{\mathcal{P}}^T}{\sqrt{d}} \right) \mathbf{V}_{\mathcal{P}}$, and $\hat{\mathbf{X}}_{\text{Att}}^{(\mathcal{H})} = \sigma \left(\frac{\mathbf{Q}_{\mathcal{H}} \mathbf{K}_{\mathcal{P}}^T}{\sqrt{d}} \right) \mathbf{V}_{\mathcal{H}}$. The number of interactions becomes drastically smaller, enabling computing $\hat{\mathbf{A}}$ with limited memory. This formulation can be seen as a sparse attention pattern [48] on a multimodal sequence, where sparsity is imposed between patch tokens. This formulation is parameter-efficient as a unique set of keys, queries, and values is learned for encoding both modalities. After passing $\hat{\mathbf{X}}_{\text{Att}}$ through a feed-forward layer with layer normalization, we take the mean representation of the post-attention pathway and patch tokens denoted as $\bar{\mathbf{x}}_{\text{Att}}^{\mathcal{P}}$ and $\bar{\mathbf{x}}_{\text{Att}}^{\mathcal{H}}$, respectively. The final representation $\bar{\mathbf{x}}_{\text{Att}}$, is then defined by the concatenation of $\bar{\mathbf{x}}_{\text{Att}}^{\mathcal{P}}$ and $\bar{\mathbf{x}}_{\text{Att}}^{\mathcal{H}}$.

D. Survival Prediction

Using the multimodal embedding $\bar{\mathbf{x}}_{\text{Att}} \in \mathbb{R}^{2d}$, our objective is to predict patient survival. Following previous work [70], we define the patient's survival state by: (1) censorship status c , where $c = 0$ represents an observed patient death and $c = 1$ corresponds to the patient's last known follow-up, and (2) a time-to-event t_i , which corresponds to the time between the patient's diagnostic and observed death if $c = 0$, or the last follow-up if $c = 1$. Instead of directly predicting the observed time of event t , we approximate it by defining non-overlapping time intervals (t_{j-1}, t_j) , $j \in [1, \dots, n]$ based on the quartiles of survival time values, and denoted as y_j . The problem simplifies to classification with censorship information, where each patient is now defined by $(\bar{\mathbf{x}}_{\text{Att}}, y_j, c)$. We build a network classifier such that each output logit predicted by the network \hat{y}_j correspond to a time interval. From there, we define the discrete hazard function $f_{\text{hazard}}(y_j | \bar{\mathbf{x}}_{\text{Att}}) = S(\hat{y}_j)$ where S is the sigmoid activation. Intuitively, $f_{\text{hazard}}(y_j | \bar{\mathbf{x}}_{\text{Att}})$ represents the probability that the patient dies during time interval (t_{j-1}, t_j) . Additionally, we define the discrete survival function $f_{\text{surv}}(y_j | \bar{\mathbf{x}}_{\text{Att}}) = \prod_{k=1}^j (1 - f_{\text{hazard}}(y_k | \bar{\mathbf{x}}_{\text{Att}}))$ that represents the probability that the patient survives up to time interval (t_{j-1}, t_j) . These enable us to define the negative

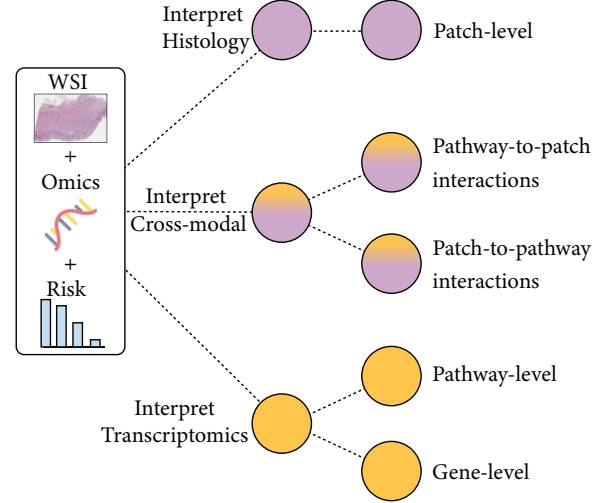


Figure 3: Proposed multi-level interpretability framework.

log-likelihood (NLL) survival loss [70], which generalizes NLL to data with censorship. Formally, we express it as:

$$\mathcal{L}(\{\bar{\mathbf{x}}_{\text{Att}}^{(i)}, y_j^{(i)}, c^{(i)}\}_{i=1}^{N_{\mathcal{D}}}) = \quad (3)$$

$$\sum_{i=1}^{N_{\mathcal{D}}} -c^{(i)} \log(f_{\text{surv}}(y_j^{(i)} | \bar{\mathbf{x}}_{\text{Att}}^{(i)})) \quad (4)$$

$$+ (1 - c^{(i)}) \log(f_{\text{surv}}(y_j^{(i)} - 1 | \bar{\mathbf{x}}_{\text{Att}}^{(i)})) \quad (5)$$

$$+ (1 - c^{(i)}) \log(f_{\text{hazard}}(y_j^{(i)} | \bar{\mathbf{x}}_{\text{Att}}^{(i)})) \quad (6)$$

where $N_{\mathcal{D}}$ is the number of samples in the dataset. Intuitively, Eq. 4 enforces a high survival probability for patients who remain alive after the final follow-up, Eq. 5 enforces that patients that died have high survival up to the time stamp where death was observed, and Eq. 6 ensures that the correct timestamp is predicted for patients for whom death is observed. A thorough mathematical description can be found in [70].

Finally, by taking the negative of the sum of all logits, we can define a patient-level risk used to identify different risk groups and stratify patients.

E. Multi-Level Interpretability

We propose an interpretability framework that operates across multiple levels, to derive transcriptomics, histology, and cross-modal interpretability (see Fig. 3).

Transcriptomics: We employ Integrated Gradient (IG) [71] to identify the influence of *pathways* and *genes*, resulting in a score describing the degree to which each pathway, respectively gene, contributes to predicting the risk. A negative IG score corresponds to a pathway/gene being associated with a lower risk, while a positive IG score indicates an association with a higher risk. A very small score denotes negligible influence. Such interpretability

analysis serves two purposes: (1) validation of known genes and pathways associated with prognosis and (2) identification of novel gene and pathway candidates that could be predictive of prognosis.

Histology: We process analogously to derive *patch-level* influence that enables studying the morphology of low and high-risk-associated patches.

Cross-modal interactions: Finally, we can study *pathway-to-patch* and *patch-to-pathway* interactions using the learned Transformer attention matrix $\hat{\mathbf{A}}$. Specifically, we define the importance of patch j (respectively pathway) with respect to pathway i (respectively patch) as $\hat{\mathbf{A}}_{ij}$ (respectively $\hat{\mathbf{A}}_{ji}$). This enables building heatmaps correlating a pathway and corresponding morphological features. This interpretability property is unique to our framework and enables studying how specific cellular functions described by a pathway interact with histology.

IV. EXPERIMENTS

A. Dataset and Implementation

We evaluate SURVPATH on five datasets from TCGA: Bladder Urothelial Carcinoma (BLCA) (n=359), Breast Invasive Carcinoma (BRCA) (n=869), Stomach Adenocarcinoma (STAD) (n=317), Colon and Rectum Adenocarcinoma (COADREAD) (n=296), and Head and Neck Squamous Cell Carcinoma (HNSC) (n=392). Prior studies have focused on predicting overall survival (OS) [60], however, this approach risks overestimating the proportion of cancer-related deaths as patients may have succumbed to other causes. Instead, we predict disease-specific survival (DSS) as a more accurate representation of the patient’s disease status.

Pathway collection: We used the Xena database [73] to access raw transcriptomics from TCGA ($N_G = 60,499$ in total) along with DSS labels. We extracted pathways from two resources: Reactome [29] and the Human Molecular Signatures Database (MSigDB) – Hallmarks [27], [28]. Reactome and MSigDB–Hallmarks comprise 1,281 and 50 human biological pathways, respectively. We further selected pathways for which at least 90% of the transcriptomics are available, resulting in 331 pathways derived from 4,999 different genes (281 Reactome pathways from 1,577 genes and 50 Hallmarks pathways from 4,241 genes).

Histology collection: We collected all diagnostic WSIs used for primary diagnosis, resulting in 2,407 WSIs with an average of 14,509 patches per WSI at 20 \times (assuming 256×256 patches). In total, we collected over 2.86 TB of raw image data, comprising around 33.8 million patches.

Implementation: We employed 5-fold cross-validation to train all models. Each split was stratified according sample collection site to mitigate potential batch artifacts [74]. Models were implemented in PyTorch, interpretability was derived with Captum [75]. To increase variability during training, we randomly sampled 4,096 patches from the WSI.

At test time, all patches were used to yield the final prediction. SURVPATH, baselines and ablations were optimized using the RAdam optimizer [76], a batch size of 1, a learning rate of 5×10^{-4} , and 10^{-3} weight decay. The patch encoder yields 768-dimensional embeddings that are projected to $d = 256$, the token dimension. The transcriptomics encoder is composed of 2-layer feed-forward networks with alpha dropout [72] to yield pathway tokens. The Transformer is implemented with a single head and layer, without class (CLS) token. The transformer is followed by a layernorm, a feed-forward layer, and a 2-layer classification head.

B. Baselines and Metrics

We group baselines into three categories: (1) unimodal histology methods, (2) unimodal transcriptomics methods, and (3) multimodal methods that are further sub-categorized into early vs. late fusion methods.

Histology baselines: All baselines use the same pre-trained feature extractor as SURVPATH [69]. We compare with *ABMIL* [14], which uses a gated-attention pooling, *AMISL* [6], which first clusters patch embeddings using K-means before attention, and *TransMIL* [15], that approximates patch self-attention with Nyström method [49].

Transcriptomics baselines: All baselines use the same input defined by aggregating Reactome and Hallmarks transcriptomics. (a) *MLP* [77] uses a 4-layer MLP, (b) *SNN* [60], [77] supplements *MLP* with additional alpha dropout layers, and (c) *S-MLP* [66], [67] uses a 2-layer sparse pathway-aware MLP followed by a dense 2-layer MLP. This baseline shares similarities with our transcriptomics encoder.

Multimodal baselines: (a) **Late fusion:** We combine *ABMIL* [14], *AMISL* [6], and *TransMIL* [15] with an S-MLP using concatenation [61], denoted as *ABMIL (Cat)*, *AMISL (Cat)*, and *TransMIL (Cat)*, and Kronecker product [60], [78]–[80], denoted as *ABMIL (KP)*, *AMISL (KP)*, and *TransMIL (KP)*. (b) **Early fusion:** *MCAT* [26] uses genomic-guided cross-attention followed by modality-specific self-attention blocks.

Metrics: The models are evaluated using (1) the concordance index (c-index, higher is better), which measures the proportion of all possible pairs of observations where the model’s predicted values correctly predict the ordering of the actual survival (ranges from 0.5 (random prediction) to 1 (perfect prediction)), and (2) Kaplan-Meier (KM) curves that enable visualizing the probability of survival of patients of different risk groups over a certain period of time. We apply the logrank statistical significance test to determine if the separation between low and high-risk groups is statistically significant (p-value < 0.05).

C. Survival Prediction Results

Table I and Table II present results of SURVPATH and baselines evaluated at 20 \times and 10 \times magnification, respectively. SURVPATH reaches best overall performance,

Table I: Results of SURVPATH and baselines in predicting disease-specific patient survival measured with c-Index (at 20x). Best performance in **bold**, second best underlined. Cat refers to concatenation, KP refers to Kronecker product. All omics and multimodal baselines were trained with the Reactome and Hallmark pathway sets.

	Model/Study	BRCA (↑)	BLCA (↑)	COADREAD (↑)	HNSC (↑)	STAD (↑)	Overall (↑)
WSI	ABMIL [14]	0.493±0.126	0.518±0.078	0.630±0.102	<u>0.580±0.019</u>	0.550±0.077	0.554
	AMISL [6]	0.500±0.000	0.500±0.000	0.500±0.000	0.518±0.015	0.506±0.014	0.508
	TransMIL [15]	0.530±0.057	0.551±0.091	0.632±0.143	0.523±0.043	0.544±0.080	0.556
Omics	MLP	0.611±0.080	<u>0.627±0.062</u>	0.625±0.060	0.548±0.045	<u>0.586±0.098</u>	<u>0.599</u>
	SNN [72]	0.528±0.094	0.584±0.113	0.521±0.109	0.550±0.065	0.565±0.080	0.550
	S-MLP [67]	0.512±0.028	0.595±0.114	0.581±0.066	0.542±0.052	0.515±0.081	0.549
Multimodal	ABMIL (Cat) [61]	0.541±0.158	0.562±0.067	0.592±0.102	<u>0.580±0.089</u>	0.523±0.098	0.560
	ABMIL (KP) [21]	0.615±0.083	0.566±0.038	0.584±0.109	0.566±0.066	0.525±0.140	0.571
	AMISL (Cat) [6]	0.462±0.179	0.518±0.055	0.510±0.137	0.478±0.051	0.538±0.025	0.501
	AMISL (KP) [6]	0.533±0.106	0.554±0.055	0.567±0.182	0.516±0.068	0.552±0.035	0.544
	TransMIL (Cat) [15]	0.598±0.087	0.630±0.047	0.539±0.189	0.542±0.091	0.536±0.090	0.569
	TransMIL (KP) [15]	0.629±0.144	0.625±0.079	0.566±0.081	0.515±0.116	0.552±0.035	0.577
	MCAT [26]	0.652±0.117	0.598±0.094	0.634±0.204	0.531±0.049	0.557±0.101	0.594
	SURVPATH (Ours)	0.655±0.089	0.625±0.056	0.673±0.170	0.600±0.061	0.592±0.047	0.629

Table II: Results of SURVPATH and baselines in predicting disease-specific patient survival measured with c-Index (at 10x). Best performance in **bold**, second best underlined. Cat refers to concatenation, KP refers to Kronecker product. All omics and multimodal baselines were trained with the Reactome and Hallmark pathway sets. The omics baselines are carried forward from the 20x experiments.

	Model/Study	BRCA (↑)	BLCA (↑)	COADREAD (↑)	HNSC (↑)	STAD (↑)	Overall (↑)
WSI	ABMIL [14]	0.604±0.110	0.518±0.078	0.652±0.192	0.572±0.070	0.522±0.136	0.574
	AMISL [6]	0.500±0.000	0.500±0.000	0.506±0.012	0.498±0.050	0.500±0.000	0.501
	TransMIL [15]	0.527±0.157	0.541±0.043	0.628±0.193	0.557±0.056	0.516±0.080	0.554
Omics	MLP	0.611±0.080	<u>0.627±0.062</u>	0.625±0.060	0.548±0.045	<u>0.586±0.098</u>	<u>0.599</u>
	SNN [72]	0.528±0.094	0.584±0.113	0.521±0.109	0.550±0.065	<u>0.565±0.080</u>	0.550
	S-MLP [67]	0.512±0.028	0.595±0.114	0.581±0.066	0.542±0.052	0.515±0.081	0.549
Multimodal	ABMIL (Cat) [61]	<u>0.623±0.066</u>	0.619±0.094	0.622±0.165	0.549±0.063	0.547±0.111	0.592
	ABMIL (KP) [21]	0.529±0.099	0.592±0.086	0.640±0.183	<u>0.596±0.039</u>	0.526±0.107	0.577
	AMISL (Cat) [6]	0.508±0.131	0.543±0.069	0.620±0.110	0.539±0.051	0.583±0.104	0.559
	AMISL (KP) [6]	0.551±0.122	0.500±0.068	0.518±0.151	0.523±0.063	0.565±0.062	0.531
	TransMIL (Cat) [15]	0.539±0.072	0.598±0.043	0.632±0.200	0.537±0.065	0.547±0.094	0.571
	TransMIL (KP) [15]	0.538±0.054	0.603±0.043	0.686±0.195	0.521±0.111	0.459±0.170	0.561
	MCAT [26]	0.473±0.123	0.545±0.070	0.480±0.243	0.494±0.072	0.433±0.064	0.485
	SURVPATH (Ours)	0.640±0.093	0.628±0.073	<u>0.675±0.175</u>	0.605±0.068	0.598±0.081	0.629

outperforming unimodal and multimodal baselines at both 20× and 10×. At 20×, SURVPATH reaches +7.3% compared to TransMIL, +3.0% compared to MLP, and +3.5 compared to MCAT. We attribute the high performance of SURVPATH to (1) the use of both modalities, (2) a unified, simple, and parameter-efficient fusion model, and (3) a semantically meaningful transcriptomics tokenizer.

Transcriptomics vs. Histology vs. Multimodal: Multimodal baselines significantly outperform histology baselines. Interestingly, a simple MLP trained on our set of transcriptomics constitutes a strong baseline that outperforms several multimodal methods. This highlights the challenge of performing robust feature selection and integrating heterogeneous and high-dimensional data modalities. In addition, the relatively small dataset size further complicates learning

of complex models.

Context vs. No context: ABMIL and TransMIL perform similarly, despite TransMIL modeling path-to-patch interactions using Nyström attention. This observation supports our design choice of disregarding patch-to-patch interactions. In addition, SURVPATH performance is similar across magnifications (0.629 overall c-index in both cases). This observation also holds for most histology and multimodal baselines.

Sparse vs. dense transcriptomics encoders: A dense MLP yields better performance than a sparse pathway-aware MLP. However, sparse networks have shown to be particularly parameter-efficient when the number of genes considered drastically increases and are more interpretable than regular MLPs [67]. As the number of genes increases,

Table III: Studying design choices for tokenization (top) and fusion (bottom) in SURVPATHat 20 \times magnification. **Top:** *Single* refers to no tokenization, using tabular transcriptomics features as a single token. *Families* refers to the set of six gene families in MutSigDB, as used in [26]. *React.+Hallmarks* refers to the main SURVPATH model reported in Table I. **Bottom:** $A_{P \rightarrow P}$ and $A_{P \leftrightarrow H}$ refers to pathway-to-pathway, pathway-to-patch, and patch-to-pathway interactions, which is the main SURVPATH model reported in Table I. \tilde{A} refers to using Nyström attention to approximate A .

Model/Study	BRCA (\uparrow)	BLCA (\uparrow)	COADREAD (\uparrow)	HNSC (\uparrow)	STAD (\uparrow)	Overall (\uparrow)
Tokenizer	Single	0.625 \pm 0.149	0.560 \pm 0.086	0.604 \pm 0.176	0.580 \pm 0.075	0.563 \pm 0.140
	Families	0.620 \pm 0.094	0.613 \pm 0.061	0.671 \pm 0.111	0.600 \pm 0.076	0.540 \pm 0.071
	Hallmarks	0.645 \pm 0.039	0.635 \pm 0.093	0.633 \pm 0.151	0.589 \pm 0.076	0.581 \pm 0.039
	Reactome	0.579 \pm 0.044	0.604 \pm 0.080	0.639 \pm 0.200	0.574 \pm 0.061	0.619 \pm 0.047
	React.+Hallmarks	0.655 \pm 0.089	0.625 \pm 0.056	0.673 \pm 0.170	0.600 \pm 0.061	0.592 \pm 0.047
Fusion	$A_{P \rightarrow P}, A_{P \rightarrow H}$	0.446 \pm 0.116	0.603 \pm 0.038	0.565 \pm 0.166	0.526 \pm 0.030	0.582 \pm 0.053
	$A_{P \rightarrow P}, A_{H \rightarrow P}$	0.546 \pm 0.118	0.589 \pm 0.037	0.633 \pm 0.130	0.498 \pm 0.037	0.480 \pm 0.083
	$A_{P \rightarrow P}, A_{H \rightarrow P}, A_{P \rightarrow H}$	0.655 \pm 0.089	0.625 \pm 0.056	0.673 \pm 0.170	0.600 \pm 0.061	0.592 \pm 0.047
	\tilde{A} [49]	0.555 \pm 0.066	0.565 \pm 0.101	0.612 \pm 0.194	0.508 \pm 0.032	0.493 \pm 0.086
						0.547

Table IV: Studying design choices for tokenization (top) and fusion (bottom) in SURVPATHat 10 \times magnification. **Top:** *Single* refers to no tokenization, using tabular transcriptomics features as a single token. *Families* refers to the set of six gene families in MutSigDB, as used in [26]. *React.+Hallmarks* refers to the main SURVPATH model reported in Table II. **Bottom:** $A_{P \rightarrow P}$ and $A_{P \leftrightarrow H}$ refers to pathway-to-pathway, pathway-to-patch, and patch-to-pathway interactions, which is the main SURVPATH model reported in Table II. \tilde{A} refers to using Nyström attention to approximate A .

Model/Study	BRCA (\uparrow)	BLCA (\uparrow)	COADREAD (\uparrow)	HNSC (\uparrow)	STAD (\uparrow)	Overall (\uparrow)
Tokenizer	Single	0.617 \pm 0.147	0.599 \pm 0.077	0.533 \pm 0.07	0.544 \pm 0.077	0.524 \pm 0.117
	Families	0.534 \pm 0.156	0.588 \pm 0.060	0.686 \pm 0.156	0.543 \pm 0.077	0.457 \pm 0.077
	Hallmarks	0.609 \pm 0.087	0.633 \pm 0.090	0.659 \pm 0.117	0.601 \pm 0.031	0.580 \pm 0.052
	Reactome	0.665 \pm 0.086	0.634 \pm 0.077	0.626 \pm 0.157	0.611 \pm 0.067	0.603 \pm 0.033
	React.+Hallmarks	0.640 \pm 0.093	0.628 \pm 0.073	0.675 \pm 0.175	0.605 \pm 0.068	0.598 \pm 0.081
Fusion	$A_{P \rightarrow P}, A_{P \rightarrow H}$	0.589 \pm 0.077	0.570 \pm 0.099	0.594 \pm 0.124	0.568 \pm 0.067	0.546 \pm 0.135
	$A_{P \rightarrow P}, A_{H \rightarrow P}$	0.573 \pm 0.085	0.577 \pm 0.118	0.531 \pm 0.221	0.566 \pm 0.064	0.521 \pm 0.056
	$A_{P \rightarrow P}, A_{H \rightarrow P}, A_{P \rightarrow H}$	0.640 \pm 0.093	0.628 \pm 0.073	0.675 \pm 0.175	0.605 \pm 0.068	0.598 \pm 0.081
	\tilde{A} [49]	0.495 \pm 0.177	0.591 \pm 0.068	0.600 \pm 0.190	0.508 \pm 0.066	0.605 \pm 0.075
						0.560

this trend might evolve.

Early vs. Late fusion: *Early fusion* methods (MCAT [26] and SURVPATH) outperform late fusion multimodal baselines at 20 \times (+5.2 for SURVPATH vs. TransMIL (KP)). We attribute this observation to the creation of a joint feature space that can model fine-grained interactions between transcriptomics and histology tokens. Overall, these findings justify the need for (1) modeling dense interactions between pathway and patch tokens and (2) unifying fusion in a single Transformer attention.

Kaplan Meier analysis: Fig. 4 shows Kaplan-Meier survival curves of predicted high-risk and low-risk groups at 20 \times . All patients with a risk higher than the median of the entire cohort are assigned as high risk (red), and patients with a risk lower than the median as low risk (blue). For all five diseases, SURVPATH highlights statistically better discrimination of the two risk groups compared to the best histology baseline (TransMIL), transcriptomics baseline (MLP), and multimodal baseline (MCAT).

D. Ablation Study

To evaluate our design choices, we performed a series of ablations studying different *Tokenizer* and *Fusion* schemes.

Tokenizer: SURVPATH employs the Reactome and Hallmarks databases as sources of biological pathways. We assess the model performance when using each database in isolation, as well as using all genes assigned to one token (*Single*) and the gene families used in [26]. With increased granularity of transcriptomics tokens, the overall performance increases, showing that building semantic tokens, not only bring interpretability properties but also improves performance. We attribute this observation to the fact that each token encodes more and more specific biological functions, enabling better cross-modal modeling.

Fusion: We ablate SURVPATH by further simplifying Transformer attention to its left part considering $A_{P \rightarrow P}$ and $A_{H \rightarrow P}$, and to its top part $A_{P \rightarrow P}$ and $A_{P \rightarrow H}$ (this design resembles MCAT [26] where a single, shared multimodal attention layer is learned). Both branches bring complementary information (observed decrease of -5.6% and -7.5% in c-index), justifying the need to model both pathway-to-patch and patch-to-pathways interactions. We further adapt

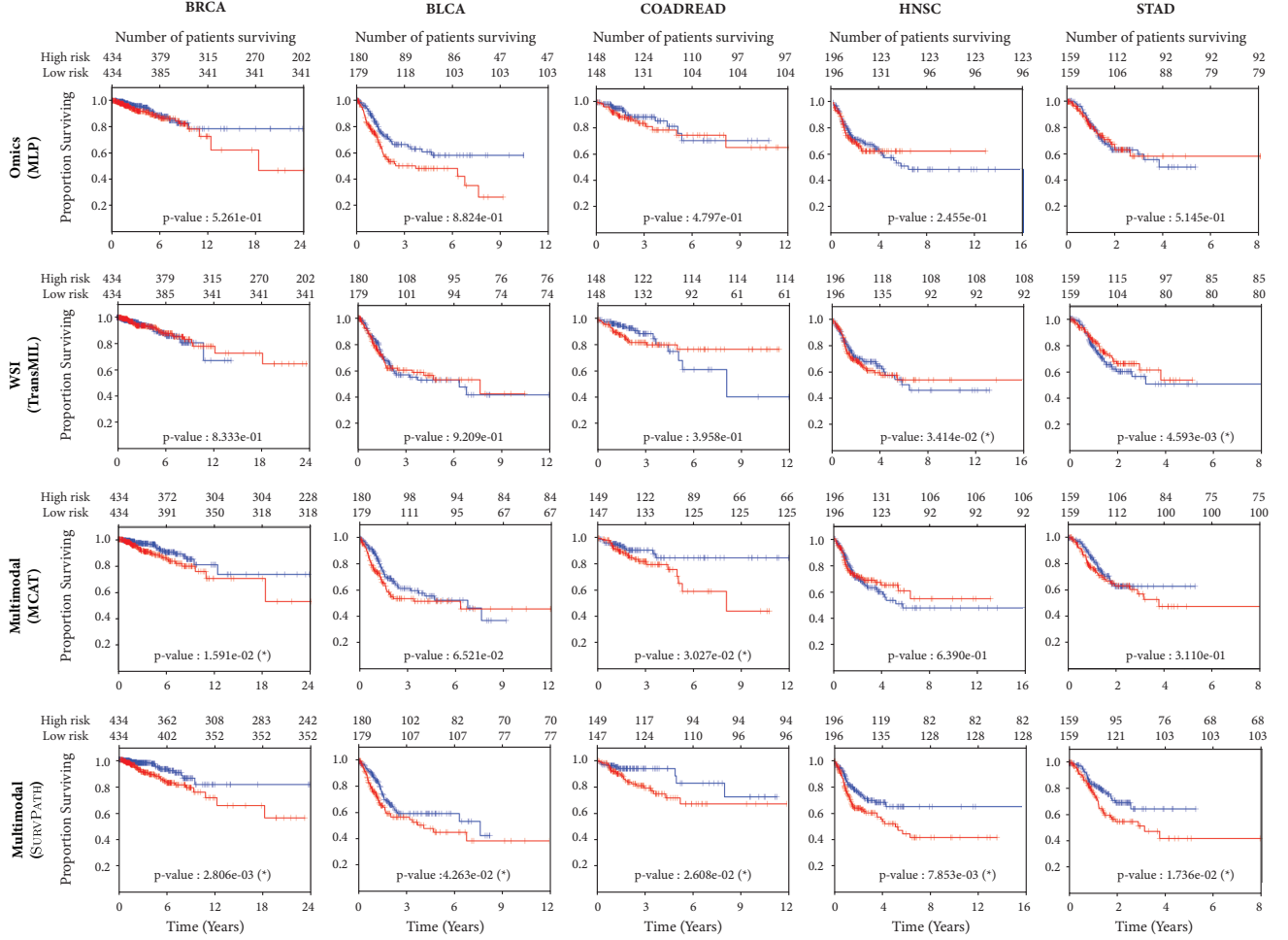


Figure 4: Kaplan Meier curves of SURVPATH, compared against histology, transcriptomics, and multimodal baselines. High (red) and low-risk (blue) groups are identified by using the median predicted risk as cut-off. Logrank test was used to determine statistical significance ($\alpha = 0.05$).

SURVPATH with Nyström attention that enables training on very long sequences by simplifying self-attention with a low-rank approximation. This yields significantly worse performance -6.9% . We hypothesize that the “true full attention” has low-entropy, making it more challenging to be approximated by low-rank methods [81], and that sparse attention patterns offer better approximations.

E. Interpretability

Examination of the multi-level interpretability can lead to novel biological insight regarding the interplay between pathways and histology in determining a patient’s risk. Here, we compare a low (top) and high (bottom) risk case of breast invasive carcinoma (BRCA) (Fig. 5) and bladder urothelial carcinoma (BLCA) (Fig. 6).

BRCA interpretability analysis: Several pathways have high absolute importance scores in the low and high-risk cases, most notably the Hallmark Epithelial-Mesenchymal

Transition (EMT) [82] and COX Reactions pathways [83], both of which are known to be involved in breast cancer. EMT is thought to underlie tumor cells’ ability to invade and metastasize [84], and the inverse importance of this pathway for the low- and high-risk cases is compatible with this analysis. This finding is enforced by studying the cross-modal interpretability that highlights the association of EMT with nests of tumor cells invading stroma. Members of the COX family of cyclooxygenases, especially COX-2, have also been implicated in breast carcinogenesis and are being investigated as a component of therapeutic regimens [85]. Cross-modal interpretability demonstrates stromal and immune cells in both cases. Though there is some overlap between important pathways in the two cases in Fig. 5, the majority differ between the two. For instance, in the high-risk case, a pathway relating to iron metabolism (a known contributor to breast carcinogenesis and prognosis [86]) was identified, with patches showing small nests of tumor

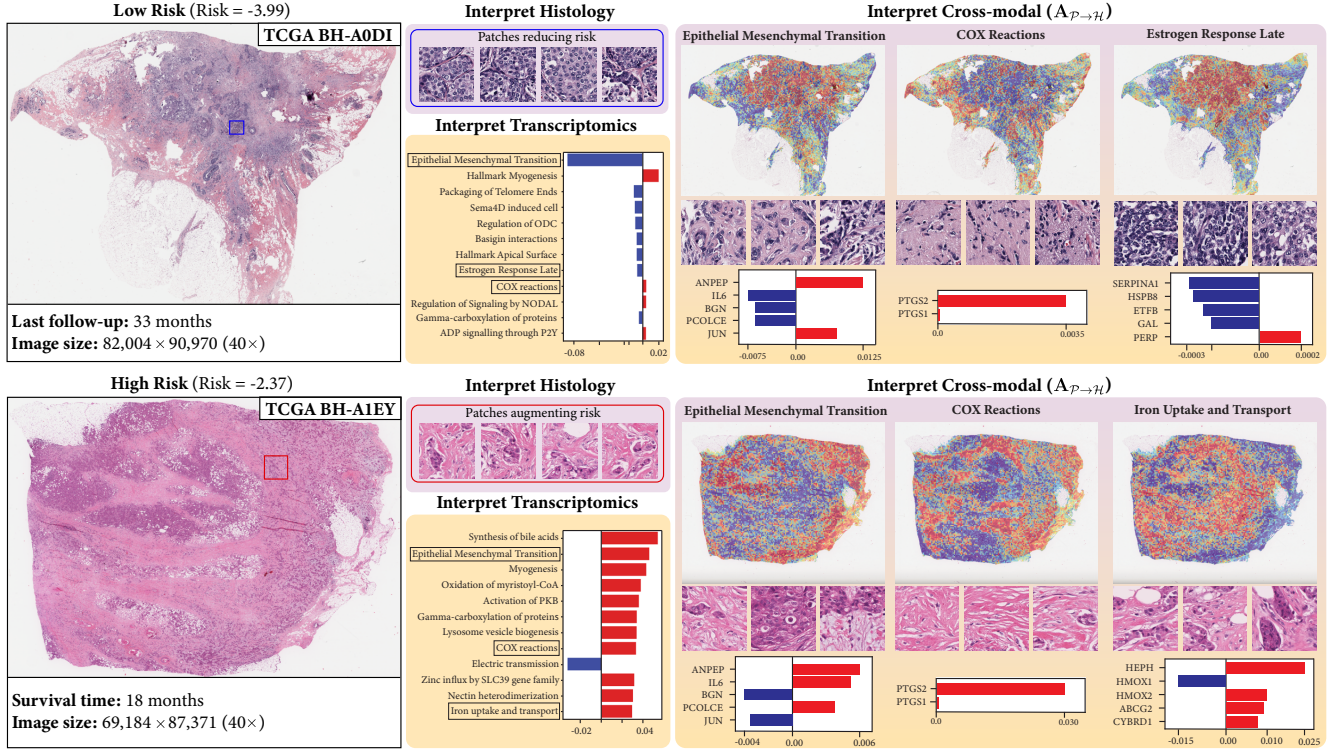


Figure 5: Multi-level interpretability visualization for breast invasive carcinoma (BRCA) including those pathways with the top integrated gradient scores for two representative cases and selected pathways from each case. **Top:** Low-risk patient. **Bottom:** High-risk patient. Genes and pathways in red increase risk and those in blue decrease risk. Heatmap colors indicate importance, with red indicating high importance and blue indicating low importance. The pathways and morphologies identified as important in these cases generally correspond well with patterns that have been previously described in invasive breast cancer (e.g. Estrogen Response Late).

cells invading through a dense stroma. In the low-risk case, a pathway relating to the cellular response to estrogen was found to be important, with corresponding patches demonstrating lower-grade invasive carcinoma or carcinoma in situ morphologies, consistent with others' observation that hormone-positive breast cancers tend to be lower grade and have longer survival times [87].

By further studying cases of estrogen receptor (ER)-positive patients in the BRCA cohort, we found that in 263 out of the 541 ER-positive patients (59%), estrogen response pathways (HALLMARK_ESTROGEN_RESPONSE_LATE and HALLMARK_ESTROGEN_RESPONSE_EARLY) are important (IG score larger than 2% of the total transcriptomics attributions). In addition, in 151 of the 263 ER-positive cases (57%), ER pathways contribute to lowering patient risk. In contrast, we find that ER pathways are important in only 42 of the 157 ER-negative patients (26%).

Interestingly, the Hallmark Myogenesis pathway is assigned relatively high positive importance for both cases in Fig. 5. Myogenesis has not been extensively studied in breast cancer, but it is plausible that tumor cells either themselves express genes involved in this pathway as part of their

epithelial-mesenchymal transition or they induce stromal cells to do so. This highlights the ability of our method to drive novel biological insight for subsequent investigation.

BLCA interpretability analysis: Histology interpretation of low and high-risk cases indicates that the presence of healthy bladder muscle reduces risk, and pleomorphic tumor cells with foamy cytoplasm contribute to augmenting risk. The majority of important pathways relate to cell cycle control (e.g., G2M checkpoint, SCF β TrCP degradation of em1), metabolism (e.g., fatty acid metabolism), and immune-related function (allograft rejection and IL2 STAT5 signaling). Previous pathway expression analyses have found G2M checkpoint and immune-related pathways to be significant in predicting bladder cancer prognosis [88]. The contributions of pathways to overall risk are also in line with previous literature. For example, allograft rejection in the low-risk case, which attends highly to tumor-infiltrating lymphocytes, reduces the risk. The allograft rejection pathway consists of multiple genes that are activated in immune response to allografts and cancer. In the low-risk case, allograft rejection highly attends to tumor-infiltrating lymphocytes and collections of lymphocytes within and near

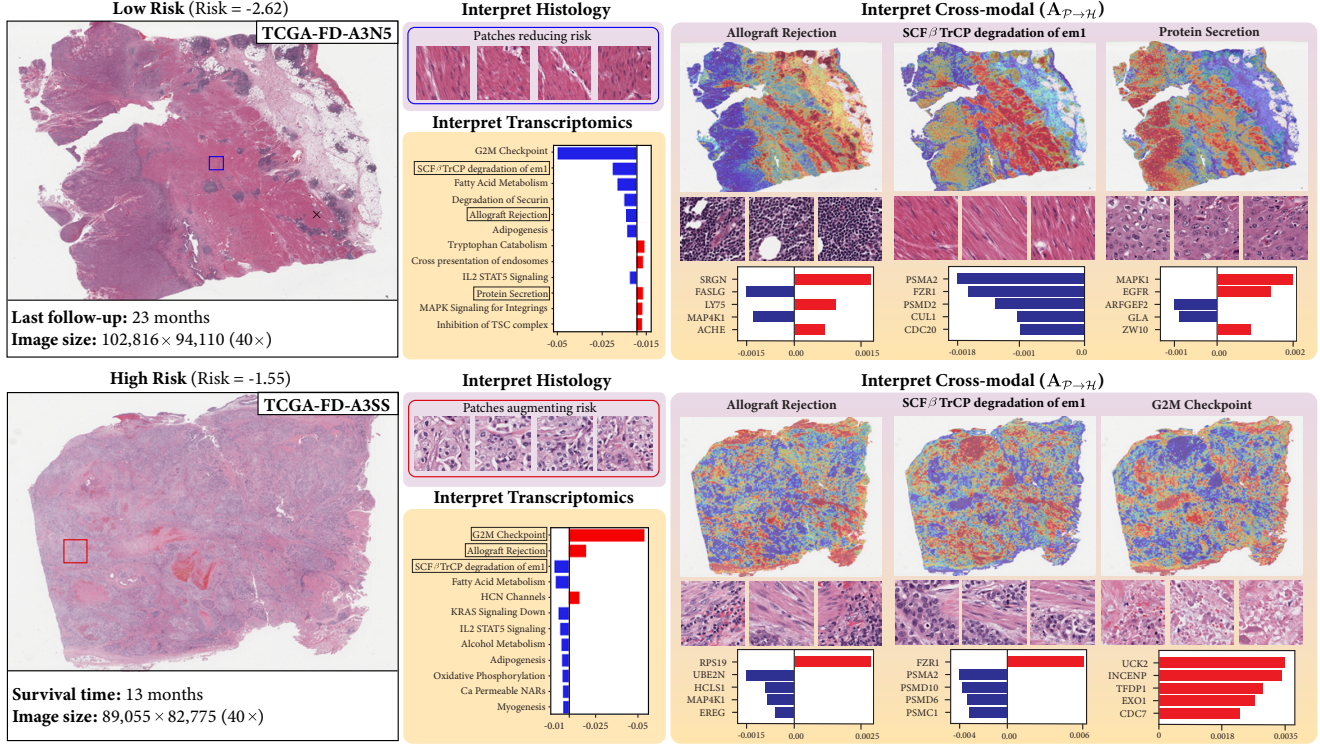


Figure 6: Multi-level interpretability visualization for bladder urothelial carcinoma (BLCA) including those pathways with the top integrated gradient scores for two representative cases and selected pathways from each case. **Top:** Low-risk patient. **Bottom:** High-risk patient. Genes and pathways in red increase risk, and those in blue decrease risk. Heatmap colors indicate importance, with red indicating high importance and blue indicating low importance. The pathways and morphologies identified as important in these cases generally correspond well with patterns that have been previously described in bladder urothelial carcinoma (e.g., the G2M checkpoint).

the muscular wall of the bladder. In the higher-risk case, this pathway again attends to collections of inflammatory cells that are interspersed within the muscular wall. The SCF β TrCP degradation of em1 pathway is important in controlling cell division by mitosis. In the low-risk case, this pathway attends to uninvolved bladder muscle, whereas in the high-risk case, the same pathway attends to tumor cells invading the bladder muscle. While there is an overlap between pathways for low and high-risk cases, SURVPATH also identifies unique pathways for the cases. For example, in the low-risk case, SURVPATH finds the protein secretion pathway to be highly attending to tumor cells and not the healthy bladder muscle cells. In both cases, the G2M checkpoint pathway (critical for the healthy progress of the cell cycle) is found to be important. In the high-risk case, we see this pathway contributing largely to increasing risk. Interestingly, we also find that this pathway attends to large areas of necrosis, which is reasonable given that aberrations in cell cycle regulation lead to cell death.

The flexibility of our approach in providing unimodal and cross-modal interpretability allows us to uncover novel

multimodal biomarkers of prognosis that could conceivably be used to design better cancer therapies. As our understanding of the molecular underpinnings of disease grows, the interpretability of SURVPATH may spur research into the possibility of targeting specific combinations of morphologies and pathways.

V. CONCLUSION

Summary: This paper addresses two major challenges posed by the multimodal fusion of transcriptomics and histology for survival prediction: (1) we address the challenge of transcriptomics tokenization by defining *biological pathway* tokens that encode semantically meaningful and interpretable cellular functions, and (2) we overcome the computational challenge of integrating long multimodal sequences by designing a multimodal Transformer with sparse modality-specific attention patterns. Our model, SURVPATH, achieves state-of-the-art survival performance when tested on five datasets from TCGA. In addition, our proposed multi-level interpretability framework reveals known and candidate prognostic features.

Limitations and future work: While our interpretability framework enables identifying prognostic features, these findings remain qualitative. Future work could be dedicated to developing interpretability metrics to generalize findings at dataset-level, *e.g.*, with quantitative morphological characterizations of specific pathway influence. In addition, our findings suggest that incorporating patch-to-patch interactions does not lead to improved performance. Nonetheless, the absence of a performance boost should not be construed as evidence that patch-to-patch interactions are unnecessary. Rather, efficiently modeling such interactions is a challenging problem that remains to be solved. Though the influence of batch artifacts was mitigated to the best of our ability via site-stratified evaluation, survival analysis in TCGA remains limited due to small sample sizes, which necessitates a community-wide effort for developing additional large survival datasets. Finally, this method is based on bulk transcriptomics, which cannot encode tumor heterogeneity. Emerging spatially-resolved technologies such as Spatial Transcriptomics [89] can be used to not only validate the histology-pathway interactions proposed by SURVPATH, but also unleash new exciting methodological opportunities for early-based fusion with histopathology.

REFERENCES

- [1] N. Coudray, P. S. Ocampo, T. Sakellaropoulos, N. Narula, M. Snuderl, D. Fenyö, A. L. Moreira, N. Razavian, and A. Tsigirgos, "Classification and mutation prediction from non-small cell lung cancer histopathology images using deep learning," *Nature Medicine*, vol. 24, no. 10, pp. 1559–1567, 2018.
- [2] P. Bandi, O. Geessink, Q. Manson, M. Van Dijk, M. Balkenhol, M. Hermesen, B. E. Bejnordi, B. Lee, K. Paeng, A. Zhong *et al.*, "From detection of individual metastases to classification of lymph node status at the patient level: the camelyon17 challenge," *IEEE transactions on medical imaging*, vol. 38, no. 2, pp. 550–560, 2018.
- [3] G. Campanella, M. G. Hanna, L. Geneslaw, A. Mirafior, V. Werneck Krauss Silva, K. J. Busam, E. Brogi, V. E. Reuter, D. S. Klimstra, and T. J. Fuchs, "Clinical-grade computational pathology using weakly supervised deep learning on whole slide images," *Nature Medicine*, 2019.
- [4] W. Bulten, K. Kartasalo, P.-H. C. Chen, P. Ström, H. Pinckaers, K. Nagpal, Y. Cai, D. F. Steiner, H. van Boven, R. Vink *et al.*, "Artificial intelligence for diagnosis and gleason grading of prostate cancer: the panda challenge," *Nature Medicine*, vol. 28, no. 1, pp. 154–163, 2022.
- [5] A. Shmatko, N. Ghaffari Laleh, M. Gerstung, and J. N. Kather, "Artificial intelligence in histopathology: enhancing cancer research and clinical oncology," *Nature Cancer*, vol. 3, no. 9, pp. 1026–1038, 2022.
- [6] J. Yao, X. Zhu, J. Jonnagaddala, N. Hawkins, and J. Huang, "Whole slide images based cancer survival prediction using attention guided deep multiple instance learning networks," *Medical Image Analysis*, vol. 65, p. 101789, 2020.
- [7] E. Wulczyn, D. Steiner, Z. Xu, A. Sadhwani, H. Wang, I. Flament, C. Mermel, P.-H. Chen, Y. Liu, and M. Stumpe, "Deep learning-based survival prediction for multiple cancer types using histopathology images," *Plos ONE*, 12 2019.
- [8] J. N. Kather, J. Krisam, P. Charoentong, T. Luedde, E. Herpel, C.-A. Weis, T. Gaiser, A. Marx, N. A. Valous, D. Ferber, L. Jansen, C. C. Reyes-Aldasoro, I. Zörnig, D. Jäger, H. Brenner, J. Chang-Claude, M. Hoffmeister, and N. Halama, "Predicting survival from colorectal cancer histology slides using deep learning: A retrospective multicenter study," *PLOS Medicine*, vol. 16, no. 1, pp. 1–22, 01 2019.
- [9] X. Wang, Y. Chen, Y. Gao, H. Zhang, Z. Guan, Z. Dong, Y. Zheng, J. Jiang, H. Yang, L. Wang, X. Huang, L. Ai, W. Yu, H. Li, C. Dong, Z. Zhou, X. Liu, and G. Yu, "Predicting gastric cancer outcome from resected lymph node histopathology images using deep learning," *Nature Communications*, vol. 12, 03 2021.
- [10] Y. Lee, J. H. Park, S. Oh, K. Shin, J. Sun, M. Jung, C. Lee, H. Kim, J.-H. Chung, K. C. Moon *et al.*, "Derivation of prognostic contextual histopathological features from whole-slide images of tumours via graph deep learning," *Nature Biomedical Engineering*, 2022.
- [11] Y. Nan, F. Li, P. Tang, G. Zhang, C. Zeng, G. Xie, Z. Liu, and G. Yang, "Automatic fine-grained glomerular lesion recognition in kidney pathology," *Pattern Recognition*, vol. 127, p. 108648, 2022.
- [12] M. S. Hosseini, L. Chan, G. Tse, M. Tang, J. Deng, S. Norouzi, C. Rowsell, K. N. Plataniotis, and S. Damaskinos, "Atlas of digital pathology: A generalized hierarchical histological tissue type-annotated database for deep learning," in *Proceedings of the IEEE/CVF Conference on Computer Vision and Pattern Recognition*, 2019, pp. 11 747–11 756.
- [13] L. Chan, M. S. Hosseini, C. Rowsell, K. N. Plataniotis, and S. Damaskinos, "Histosegnet: Semantic segmentation of histological tissue type in whole slide images," in *Proceedings of the IEEE/CVF International Conference on Computer Vision*, 2019, pp. 10 662–10 671.
- [14] M. Ilse, J. Tomczak, and M. Welling, "Attention-based deep multiple instance learning," in *International conference on machine learning*. PMLR, 2018, pp. 2127–2136.
- [15] Z. Shao, H. Bian, Y. Chen, Y. Wang, J. Zhang, X. Ji *et al.*, "Transmil: Transformer based correlated multiple instance learning for whole slide image classification," *Advances in Neural Information Processing Systems*, vol. 34, pp. 2136–2147, 2021.
- [16] R. Li, X. Wu, A. Li, and M. Wang, "HFBSurv: hierarchical multimodal fusion with factorized bilinear models for cancer survival prediction," *Bioinformatics*, vol. 38, no. 9, pp. 2587–2594, 02 2022.
- [17] Z. Wang, R. Li, M. Wang, and A. Li, "GPDBN: deep bilinear network integrating both genomic data and pathological images for breast cancer prognosis prediction," *Bioinformatics*, vol. 37, no. 18, pp. 2963–2970, 03 2021.

- [18] B. Györfy, “Survival analysis across the entire transcriptome identifies biomarkers with the highest prognostic power in breast cancer,” *Computational and Structural Biotechnology Journal*, vol. 19, pp. 4101–4109, 2021.
- [19] Á. Nagy, G. Munkácsy, and B. Györfy, “Pancancer survival analysis of cancer hallmark genes,” *Scientific Reports*, vol. 11, 2020.
- [20] S. Raghavan, P. S. Winter, A. W. Navia, H. L. Williams, A. DenAdel, K. E. Lowder, J. Galvez-Reyes, R. L. Kalekar, N. Mulugeta, K. S. Kapner, M. S. Raghavan, A. A. Borah, N. Liu, S. A. Väyrynen, A. D. Costa, R. W. Ng, J. Wang, E. K. Hill, D. Y. Ragon, L. K. Brais, A. M. Jaeger, L. F. Spurr, Y. Y. Li, A. D. Cherniack, M. A. Booker, E. F. Cohen, M. Y. Tolstorukov, I. Wakiro, A. Rotem, B. E. Johnson, J. M. McFarland, E. T. Sicinska, T. E. Jacks, R. J. Sullivan, G. I. Shapiro, T. E. Clancy, K. Perez, D. A. Rubinson, K. Ng, J. M. Cleary, L. Crawford, S. R. Manalis, J. A. Nowak, B. M. Wolpin, W. C. Hahn, A. J. Aguirre, and A. K. Shalek, “Microenvironment drives cell state, plasticity, and drug response in pancreatic cancer,” *Cell*, vol. 184, no. 25, pp. 6119–6137.e26, 2021.
- [21] R. J. Chen, M. Y. Lu, D. F. Williamson, T. Y. Chen, J. Lipkova, Z. Noor, M. Shaban, M. Shady, M. Williams, B. Joo, and F. Mahmood, “Pan-cancer integrative histology-genomic analysis via multimodal deep learning,” *Cancer Cell*, vol. 40, no. 8, pp. 865–878, Aug 2022.
- [22] A. Radford, J. W. Kim, C. Hallacy, A. Ramesh, G. Goh, S. Agarwal, G. Sastry, A. Askell, P. Mishkin, J. Clark, G. Krueger, and I. Sutskever, “Learning transferable visual models from natural language supervision,” in *Proceedings of the 38th International Conference on Machine Learning*, ser. Proceedings of Machine Learning Research, M. Meila and T. Zhang, Eds., vol. 139. PMLR, 18–24 Jul 2021, pp. 8748–8763.
- [23] J.-B. Alayrac, J. Donahue, P. Luc, A. Miech, I. Barr, Y. Hasson, K. Lenc, A. Mensch, K. Millican, M. Reynolds *et al.*, “Flamingo: a visual language model for few-shot learning,” *arXiv preprint arXiv:2204.14198*, 2022.
- [24] W. Wang, H. Bao, L. Dong, J. Bjorck, Z. Peng, Q. Liu, K. Aggarwal, O. K. Mohammed, S. Singhal, S. Som *et al.*, “Image as a foreign language: Beit pretraining for all vision and vision-language tasks,” *arXiv preprint arXiv:2208.10442*, 2022.
- [25] P. P. Liang, A. Zadeh, and L.-P. Morency, “Foundations and recent trends in multimodal machine learning: Principles, challenges, and open questions,” *arXiv preprint arXiv:2209.03430*, 2022.
- [26] R. J. Chen, M. Y. Lu, W.-H. Weng, T. Y. Chen, D. F. Williamson, T. Manz, M. Shady, and F. Mahmood, “Multimodal co-attention transformer for survival prediction in gigapixel whole slide images,” in *Proceedings of the IEEE/CVF International Conference on Computer Vision*, 2021, pp. 4015–4025.
- [27] A. Subramanian, P. Tamayo, V. K. Mootha, S. Mukherjee, B. L. Ebert, M. A. Gillette, A. Paulovich, S. L. Pomeroy, T. R. Golub, E. S. Lander, and J. P. Mesirov, “Gene set enrichment analysis: A knowledge-based approach for interpreting genome-wide expression profiles,” *Proceedings of the National Academy of Sciences*, vol. 102, no. 43, pp. 15 545–15 550, 2005.
- [28] A. Liberzon, C. Birger, H. Thorvaldsdóttir, M. Ghandi, J. P. Mesirov, and P. Tamayo, “The molecular signatures database (msigdb) hallmark gene set collection,” *Cell systems*, vol. 1, pp. 417–425, 2015.
- [29] M. Gillespie, B. Jassal, R. Stephan, M. Milacic, K. Rothfels, A. Senff-Ribeiro, J. Griss, C. Sevilla, L. Matthews, C. Gong, C. Deng, T. Varusai, E. Ragueneau, Y. Haider, B. May, V. Shamovsky, J. Weiser, T. Brunson, N. Sanati, L. Beckman, X. Shao, A. Fabregat, K. Sidiropoulos, J. Murillo, G. Viteri, J. Cook, S. Shorser, G. Bader, E. Demir, C. Sander, R. Haw, G. Wu, L. Stein, H. Hermjakob, and P. D’Eustachio, “The reactome pathway knowledgebase 2022,” *Nucleic Acids Research*, vol. 50, no. D1, pp. D687–D692, 11 2021.
- [30] Y. Wang and B. P. Zhou, “Epithelial-mesenchymal transition—a hallmark of breast cancer metastasis,” *Cancer hallmarks*, vol. 1, no. 1, pp. 38–49, 2013.
- [31] A. Vaswani, N. Shazeer, N. Parmar, J. Uszkoreit, L. Jones, A. N. Gomez, L. Kaiser, and I. Polosukhin, “Attention Is All You Need,” in *Neural Information Processing Systems (NeurIPS)*, 2017.
- [32] A. Jaegle, F. Gimeno, A. Brock, O. Vinyals, A. Zisserman, and J. Carreira, “Perceiver: General perception with iterative attention,” in *Proceedings of the 38th International Conference on Machine Learning*, ser. Proceedings of Machine Learning Research, M. Meila and T. Zhang, Eds., vol. 139, 18–24 Jul 2021, pp. 4651–4664.
- [33] A. Jaegle, S. Borgeaud, J.-B. Alayrac, C. Doersch, C. Ionescu, D. Ding, S. Koppula, D. Zoran, A. Brock, E. Shelhamer, O. J. Henaff, M. Botvinick, A. Zisserman, O. Vinyals, and J. Carreira, “Perceiver IO: A general architecture for structured inputs & outputs,” in *International Conference on Learning Representations*, 2022.
- [34] X. Zhu, J. Yao, F. Zhu, and J. Huang, “Wsa: Making survival prediction from whole slide histopathological images,” in *Proceedings of the IEEE Conference on Computer Vision and Pattern Recognition (CVPR)*, July 2017.
- [35] S. Wetstein, V. Jong, N. Stathonikos, M. Opdam, G. Dackus, J. Pluim, P. Diest, and M. Veta, “Deep learning-based breast cancer grading and survival analysis on whole-slide histopathology images,” *Scientific Reports*, vol. 12, p. 15102, 09 2022.
- [36] C. C. Mackenzie, M. Dawood, S. Graham, M. Eastwood, and F. ul Amir Afsar Minhas, “Neural graph modelling of whole slide images for survival ranking,” in *The First Learning on Graphs Conference*, 2022.
- [37] D. Di, C. Zou, Y. Feng, H. Zhou, R. Ji, Q. Dai, and Y. Gao, “Generating hypergraph-based high-order representations of whole-slide histopathological images for survival prediction,” *IEEE Transactions on Pattern Analysis and Machine Intelligence*, vol. PP, pp. 1–16, 09 2022.

- [38] Y. Schirris, E. Gavves, I. Nederlof, H. M. Horlings, and J. Teuwen, "Deepsmile: Contrastive self-supervised pre-training benefits msi and hrd classification directly from h&e whole-slide images in colorectal and breast cancer," *Medical Image Analysis*, vol. 79, p. 102464, 2022.
- [39] H. Liu and T. Kurc, "Deep learning for survival analysis in breast cancer with whole slide image data," *Bioinformatics*, vol. 38, no. 14, pp. 3629–3637, 06 2022.
- [40] Y.-H. H. Tsai, S. Bai, P. P. Liang, J. Z. Kolter, L.-P. Morency, and R. Salakhutdinov, "Multimodal transformer for unaligned multimodal language sequences," in *Proceedings of the 57th Annual Meeting of the Association for Computational Linguistics*. Florence, Italy: Association for Computational Linguistics, Jul. 2019, pp. 6558–6569.
- [41] P. Xu, X. Zhu, and D. Clifton, "Multimodal learning with transformers: A survey," 06 2022.
- [42] F. Shamshad, S. H. Khan, S. W. Zamir, M. H. Khan, M. Hayat, F. S. Khan, and H. Fu, "Transformers in medical imaging: A survey," *ArXiv*, vol. abs/2201.09873, 2022.
- [43] A. Dosovitskiy, L. Beyer, A. Kolesnikov, D. Weissenborn, X. Zhai, T. Unterthiner, M. Dehghani, M. Minderer, G. Heigold, S. Gelly *et al.*, "An image is worth 16x16 words: Transformers for image recognition at scale," in *International Conference on Learning Representations*, 2021.
- [44] J. Lin, A. Yang, Y. Zhang, J. Liu, J. Zhou, and H. Yang, "Interbert: Vision-and-language interaction for multi-modal pretraining," *ArXiv*, vol. abs/2003.13198, 2020.
- [45] K. Nguyen and T. Okatani, "Improved fusion of visual and language representations by dense symmetric co-attention for visual question answering," in *IEEE/CVF Conference on Computer Vision and Pattern Recognition (CVPR)*, 06 2018, pp. 6087–6096.
- [46] J. Lu, D. Batra, D. Parikh, and S. Lee, "Vilbert: Pretraining task-agnostic visiolinguistic representations for vision-and-language tasks," in *Proceedings of the 33rd International Conference on Neural Information Processing Systems*. Red Hook, NY, USA: Curran Associates Inc., 2019.
- [47] V. Murahari, D. Batra, D. Parikh, and A. Das, "Large-scale pretraining for visual dialog: A simple state-of-the-art baseline," in *Computer Vision – ECCV 2020*, A. Vedaldi, H. Bischof, T. Brox, and J.-M. Frahm, Eds. Cham: Springer International Publishing, 2020, pp. 336–352.
- [48] I. Beltagy, M. E. Peters, and A. Cohan, "Longformer: The long-document transformer," *arXiv:2004.05150*, 2020.
- [49] Y. Xiong, Z. Zeng, R. Chakraborty, M. Tan, G. Fung, Y. Li, and V. Singh, "Nyströmformer: A nyström-based algorithm for approximating self-attention," in *Proceedings of the AAAI Conference on Artificial Intelligence*, 2021.
- [50] K. Choromanski, V. Likhoshesterov, D. Dohan, X. Song, A. Gane, T. Sarlós, P. Hawkins, J. Davis, A. Mohiuddin, L. Kaiser, D. Belanger, L. J. Colwell, and A. Weller, "Re-thinking attention with performers," in *ICLR*, 2021.
- [51] H. Wu, J. Wu, J. Xu, J. Wang, and M. Long, "Flowformer: Linearizing transformers with conservation flows," in *International Conference on Machine Learning*, 2022.
- [52] W. Hua, Z. Dai, H. Liu, and Q. Le, "Transformer quality in linear time," in *Proceedings of the 39th International Conference on Machine Learning*, ser. Proceedings of Machine Learning Research, K. Chaudhuri, S. Jegelka, L. Song, C. Szepesvari, G. Niu, and S. Sabato, Eds., vol. 162. PMLR, 17–23 Jul 2022, pp. 9099–9117.
- [53] J. Lu, J. Yao, J. Zhang, X. Zhu, H. Xu, W. Gao, C. Xu, T. Xiang, and L. Zhang, "Soft: Softmax-free transformer with linear complexity," in *NeurIPS*, 2021.
- [54] A. Nagrani, S. Yang, A. Arnab, A. Jansen, C. Schmid, and C. Sun, "Attention bottlenecks for multimodal fusion," in *Advances in Neural Information Processing Systems*, M. Ranzato, A. Beygelzimer, Y. Dauphin, P. Liang, and J. W. Vaughan, Eds., vol. 34. Curran Associates, Inc., 2021, pp. 14 200–14 213.
- [55] J. Qiu, H. Ma, O. Levy, W.-t. Yih, S. Wang, and J. Tang, "Blockwise self-attention for long document understanding," in *Findings of the Association for Computational Linguistics: EMNLP 2020*. Online: Association for Computational Linguistics, Nov. 2020, pp. 2555–2565.
- [56] P. P. Liang, Y. Lyu, G. Chhablani, N. Jain, Z. Deng *et al.*, "Multiviz: Towards visualizing and understanding multimodal models," in *ICLR*, 2023.
- [57] X. Wang, J. He, Z. Jin *et al.*, "M2lens: Visualizing and explaining multimodal models for sentiment analysis," *IEEE Transactions on Visualization and Computer Graphics*, 2021.
- [58] E. Aflalo, M. Du, S.-Y. Tseng, Y. Liu, C. Wu, N. Duan, and V. Lal, "VI-interpret: An interactive visualization tool for interpreting vision-language transformers," in *CVPR*, 2022, pp. 21 406–21 415.
- [59] L. A. Vale-Silva and K. Rohr, "Multisurv: Long-term cancer survival prediction using multimodal deep learning," *medRxiv*, 2020.
- [60] R. J. Chen, M. Y. Lu, J. Wang, D. F. Williamson, S. J. Rodig, N. I. Lindeman, and F. Mahmood, "Pathomic fusion: an integrated framework for fusing histopathology and genomic features for cancer diagnosis and prognosis," *IEEE Transactions on Medical Imaging*, vol. 41, no. 4, pp. 757–770, 2020.
- [61] P. Mobadersany, S. Yousefi, M. Amgad, D. A. Gutman, J. S. Barnholtz-Sloan, J. E. Velázquez Vega, D. J. Brat, and L. A. Cooper, "Predicting cancer outcomes from histology and genomics using convolutional networks," *Proceedings of the National Academy of Sciences*, vol. 115, no. 13, pp. E2970–E2979, 2018.
- [62] A. Cheerla and O. Gevaert, "Deep learning with multimodal representation for pancancer prognosis prediction," *Bioinformatics*, vol. 35, no. 14, pp. i446–i454, 07 2019.
- [63] L. Qiu, A. Khormali, and K. Liu, "Deep biological pathway informed pathology-genomic multimodal survival prediction," 2023.

- [64] L. Zhuang, J. Lipkova, R. Chen, and F. Mahmood, "Deep learning-based integration of histology, radiology, and genomics for improved survival prediction in glioma patients," in *Medical Imaging 2022: Digital and Computational Pathology*, J. E. Tomaszewski, A. D. Ward, and R. M. L. M.D., Eds., vol. 12039, International Society for Optics and Photonics. SPIE, 2022, p. 120390Z.
- [65] J. Ma, M. K. Yu, S. H. Fong, K. Ono, E. Sage, B. Demchak, R. Sharan, and T. Ideker, "Using deep learning to model the hierarchical structure and function of a cell," *Nature methods*, vol. 15, pp. 290 – 298, 2018.
- [66] J. Hao, Y. Kim, T.-K. Kim, and M. Kang, "Pasnet: Pathway-associated sparse deepneural network for prognosis prediction from high-throughput data," *BMC Bioinformatics*, vol. 19, 12 2018.
- [67] H. A. Elmarakeby, J. Hwang, R. Arafeh, J. Crowdis, S. Gang, D. Liu, S. H. AIDubayan, K. Salari, S. Kregel, C. Richter *et al.*, "Biologically informed deep neural network for prostate cancer discovery," *Nature*, vol. 598, no. 7880, pp. 348–352, 2021.
- [68] X. Wang, S. Yang, J. Zhang, M. Wang, J. Zhang, W. Yang, J. Huang, and X. Han, "Transformer-based unsupervised contrastive learning for histopathological image classification," *Medical Image Analysis*, 2022.
- [69] X. Wang, S. Yang, J. Zhang, M. Wang, J. Zhang, J. Huang, W. Yang, and X. Han, "Transpath: Transformer-based self-supervised learning for histopathological image classification," in *International Conference on Medical Image Computing and Computer-Assisted Intervention*. Springer, 2021, pp. 186–195.
- [70] S. G. Zadeh and M. Schmid, "Bias in cross-entropy-based training of deep survival networks," *IEEE Transactions on Pattern Analysis and Machine Intelligence*, vol. 43, no. 9, pp. 3126–3137, 2021.
- [71] M. Sundararajan, A. Taly, and Q. Yan, "Axiomatic attribution for deep networks," in *Proceedings of the 34th International Conference on Machine Learning - Volume 70*, ser. ICML'17. JMLR.org, 2017, p. 3319–3328.
- [72] G. Klambauer, T. Unterthiner, A. Mayr, and S. Hochreiter, "Self-normalizing neural networks," in *Proceedings of the 31st International Conference on Neural Information Processing Systems*, ser. NIPS'17. Red Hook, NY, USA: Curran Associates Inc., 2017, p. 972–981.
- [73] M. J. Goldman, B. Craft, M. Hastie, K. Repečka, F. McDade, A. Kamath, A. Banerjee, Y. Luo, D. Rogers, A. N. Brooks, J. Zhu, and D. Haussler, "Visualizing and interpreting cancer genomics data via the xena platform," *Nature biotechnology*, vol. 38, no. 6, pp. 675–678, 2020.
- [74] F. Howard, J. Dolezal, S. Kochanny, J. Schulte, H. Chen, L. Heij, D. Huo, R. Nanda, O. Olopade, J. Kather, N. Cipriani, R. Grossman, and A. Pearson, "The impact of site-specific digital histology signatures on deep learning model accuracy and bias," *Nature Communications*, vol. 12, 07 2021.
- [75] N. Kokhlikyan, V. Miglani, M. Martin, E. Wang, B. Alsallakh, J. Reynolds, A. Melnikov, N. Kliushkina, C. Araya, S. Yan, and O. Reblitz-Richardson, "Captum: A unified and generic model interpretability library for pytorch," 2020.
- [76] L. Liu, H. Jiang, P. He, W. Chen, X. Liu, J. Gao, and J. Han, "On the variance of the adaptive learning rate and beyond," *arXiv preprint arXiv:1908.03265*, 2019.
- [77] S. Haykin, *Neural networks: a comprehensive foundation*. Prentice Hall PTR, 1994.
- [78] A. Fukui, D. H. Park, D. Yang, A. Rohrbach, T. Darrell, and M. Rohrbach, "Multimodal compact bilinear pooling for visual question answering and visual grounding," *arXiv preprint arXiv:1606.01847*, 2016.
- [79] A. Zadeh, M. Chen, S. Poria, E. Cambria, and L.-P. Morency, "Tensor fusion network for multimodal sentiment analysis," *arXiv preprint arXiv:1707.07250*, 2017.
- [80] W.-H. Weng, Y. Cai, A. Lin, F. Tan, and P.-H. C. Chen, "Multimodal multitask representation learning for pathology biobank metadata prediction," *arXiv preprint arXiv:1909.07846*, 2019.
- [81] B. Chen, T. Dao, E. Winsor, Z. Song, A. Rudra, and C. Ré, "Scatterbrain: Unifying sparse and low-rank attention," in *Advances in Neural Information Processing Systems*, A. Beygelzimer, Y. Dauphin, P. Liang, and J. W. Vaughan, Eds., 2021.
- [82] Y. Wang and B. P. Zhou, "Epithelial-mesenchymal transition—a hallmark of breast cancer metastasis," *Cancer hallmarks*, vol. 1 1, pp. 38–49, 2013.
- [83] D. Mazhar, R. Ang, and J. Waxman, "Cox inhibitors and breast cancer," *British journal of cancer*, vol. 94, pp. 346–50, 03 2006.
- [84] R. Kalluri, R. A. Weinberg *et al.*, "The basics of epithelial-mesenchymal transition," *The Journal of clinical investigation*, vol. 119, no. 6, pp. 1420–1428, 2009.
- [85] R. E. Harris, B. C. Casto, and Z. M. Harris, "Cyclooxygenase-2 and the inflammation of breast cancer," *World journal of clinical oncology*, vol. 5, no. 4, p. 677, 2014.
- [86] S. V. Torti and F. M. Torti, "Cellular iron metabolism in prognosis and therapy of breast cancer," *Critical Reviews™ in Oncogenesis*, vol. 18, no. 5, 2013.
- [87] L. K. Dunnwald, M. A. Rossing, and C. I. Li, "Hormone receptor status, tumor characteristics, and prognosis: a prospective cohort of breast cancer patients," *Breast cancer research*, vol. 9, pp. 1–10, 2007.
- [88] X. Jiang, Y. Xia, H. Meng, Y. Liu, J. Cui, H. Huang, G. Yin, and B. Shi, "Identification of a nuclear mitochondrial-related multi-genes signature to predict the prognosis of bladder cancer," *Frontiers in Oncology*, vol. 11, p. 746029, 2021.
- [89] L. Tian, F. Chen, and E. Z. Macosko, "The expanding vistas of spatial transcriptomics," *Nature Biotechnology*, pp. 1–10, 2022.